Research article

SPECTROSCOPY

Received: 15 October 2012 Revised: 28 December 2012 Accepted: 6 January 2013 Published online in Wiley Online Library: 31 March 2013

(wileyonlinelibrary.com) DOI 10.1002/jrs.4257

Polarized micro-Raman spectroscopy and *ab initio* phonon modes calculations of $LuPO_4$†

A. Sanson,[a] M. Giarola,[b]* M. Bettinelli,[c] A. Speghini[c] and G. Mariotto[b]

The vibrational dynamics of lutetium orthophosphate ($LuPO_4$) single crystals was carefully investigated by means of polarized micro-Raman spectroscopy and *ab initio* calculations. Eleven of the twelve independent components of the polarizability tensor, expected on the basis of the group theory for $LuPO_4$, were selected in turn and assigned in symmetry. The only $B_{1g}(2)$ Raman mode was not observed, likewise due to either its very small intensity or its nearness in energy with forbidden Raman modes, which spill and could hide it. Both Raman and infrared vibrational modes are evaluated by density-functional theory calculations using effective core pseudo-potential. The agreement between calculated and experimental frequencies is very good. On the basis of our *ab initio* results, and of reduced-mass ratio considerations, the expected wavenumber of the missing B_{1g} (2) mode falls close to that of $E_g(3)$ mode peaked at about 306 cm^{-1}, and therefore we can definitively conclude that the observation of the missing B_{1g} (2) mode is masked by the spill-over of this E_g mode.

Keywords: lutetium orthophosphate; zircon-type structure; vibrational dynamics; polarized Raman scattering; ab initio calculations

Introduction

Lutetium orthophosphate ($LuPO_4$) belongs to the family of rare-earth orthophosphates RPO_4 which can crystallize either in the monoclinic monazite structure, (for R = La–Gd), or in the tetragonal xenotime structure, (for R = Tb–Lu). These materials have attracted an increasing level of interest in recent years owing to their potential technological applications, exploiting their chemico-physical properties. In fact, in one side, the high melting temperature, structural and chemical stability, long-term corrosion, and radiation-damage resistance of these compounds suggested their use as efficient materials for nuclear waste storage.[1,2] On the other hand, orthophosphates have good optical quality, high hardness, and large refractive index, which make them the ideal candidates in relationship to their use as x-ray and gamma-ray scintillators for medical imaging applications.[3,4] The structural and physical-chemical properties of the orthophosphates, together with the wide variety of possible applications, have been recently reviewed at a very wide extent by L.A. Boatner.[5]

$LuPO_4$ crystallizes in the tetragonal zircon-type structure (space group I41/amd), in which phosphorus is in fourfold coordination with oxygen forming isolated tetrahedra joined in edge-sharing chains parallel to the crystallographic c-axis. The PO_4 tetrahedra alternate eight-fold coordination polyhedra centred on the Lu ion. The structure is stable at ambient conditions. However, a pressure-induced irreversible phase transition to the scheelite-type structure is observed in $LuPO_4$ as well as in other orthophosphates with zircon-type structure.[6–8] To achieve a complete understanding of the optical and thermodynamic behaviour of these host materials, it is important to gain information regarding their vibrational properties. However, despite the numerous experimental and theoretical studies,[9–15] the vibrational dynamics of this family of compounds is not yet fully clarified. In particular, only very recently, all the 12 independent components of the Raman polarizability tensor, expected on the basis of the group theory, were selected in turn and assigned in symmetry for both YPO_4 and $ScPO_4$ crystals, definitively overcoming the existing ambiguities and errors in the attribution of their observed Raman modes.[16] As for $LuPO_4$, at best 11 of the 12 expected Raman modes have been observed and reported. Therefore, further investigations, both experimental and theoretical, are mandatory.

In this work, we report on the results of new polarized Raman measurements performed on $LuPO_4$ single crystals, and of the vibrational dynamics calculations carried out, to the best of our knowledge for the first time, by means of an *ab initio* method. An overall, very good agreement between calculated and experimentally observed frequencies is achieved, and, on the basis of our results, we can definitively infer that the missing $B_{1g}(2)$ mode is hidden by the $E_g(3)$ mode peaked at about 306 cm^{-1}.

Experimental details

$LuPO_4$ single crystals were grown by spontaneous nucleation using a $PbO–P_2O_5$ flux (1:1 molar ratio).[5,17] The batch composition was 50 mol% $NH_4H_2PO_4$, 48 mol% PbO (Aldrich, 99.9 %),

* *Correspondence to: M. Giarola, Department of Computer Science, University of Verona, Verona, Italy*
E-mail: marco.giarola@univr.it

† *This article is from the GISR part of the joint special issue on the European Conference on Nonlinear Optical Spectroscopy (ECONOS 2012) with Guest Editors Johannes Kiefer and Peter Radi and the II Italian Conference of the National Group of Raman Spectroscopy and Non-Linear Effects (GISR 2012) with Guest Editor Maria Grazia Giorgini.*

a *Dipartimento di Fisica e Astronomia 'G. Galilei', Università di Padova, Via Marzolo 8, I-35131, Padova, Italy*

b *Dipartimento di Informatica, Università di Verona, Strada Le Grazie 15, I-37134, Verona, Italy*

c *Dipartimento di Biotecnologie, Università di Verona and INSTM, UdR Verona, Strada Le Grazie 15, I-37134, Verona, Italy*

and 2 mol% Lu_2O_3 (Aldrich, 99.99 %). The batch was put in Pt crucible and heat treated in air at 1300 °C for 15 h, and then the temperature was lowered to 800 °C with a rate of 1.8 °C/h. After the crystal growth, the flux was dissolved using hot diluted nitric acid. Single crystals of good optical quality, elongated in the direction of c-axis of the tetragonal structure, were obtained.

Polarized micro-Raman spectra were excited by the 514.5 nm or, alternatively, by the 568.2 nm line excitation. The spectra were carried out at room temperature ether in backscattering or 90° geometry from a high optical quality single crystal using a triple-axis monochromator (Horiba-Jobin Yvon, model T64000), set in double-subtractive/single configuration, and equipped with holographic gratings having 1800 lines/mm, and were detected by a charge coupled device detector, with 1024×256 pixels, cooled by liquid nitrogen. Proper orientation of the single crystal was achieved using a micro-manipulator operated under direct optical inspection of a colour camera interfaced to the microscope objective used to collect the scattered radiation. All the spectra were calibrated in wavenumber using some emission lines of a Ne spectral lamp assumed as reference. More experimental details are given in Ref.[16]

Following Porto's notation,[18] we hereafter indicate the scattering configurations as $\mathbf{k}_i(\mathbf{e}_i,\mathbf{e}_s)\mathbf{k}_s$, where $\mathbf{k}_i$ and $\mathbf{k}_s$ are the propagation directions of the incident and scattered light, respectively, $\mathbf{e}_i$ and $\mathbf{e}_s$ are the corresponding electric field directions. In reference to *X*, *Y*, *Z* axes of the laboratory coordinate frame (L system), the *Z*-axis coincides with the optical axis of the objective used to collect the scattered radiation, while, in the case of measurements under the 90° scattering geometry, the *X*-axis is coincident with the optical axis of the objective used to focus the incident radiation. According to the above mentioned notation, the scattering configurations Z′(X,X)Z, Z′(X,Y)Z, Z′(Y,Y)Z, and Z′(Y,X)Z, where Z′ = −Z, can be selectively probed in 180° scattering geometry, while the scattering configurations X(Z,Y)Z, X(Z,X)Z, X(Y,Y)Z and X(YX)Z can be selected in 90° geometry.

Polarized Raman spectra

$LuPO_4$, likewise YPO_4 and $ScPO_4$, crystallizes in the tetragonal system and belongs to space group D_{4h}^{19} ($I4_1/amd$), with two $LuPO_4$ formula units in primitive cell.[19] The 12 atoms of the primitive cell give rise to 33 optical modes at the Γ point of the Brillouin zone. Among them, 12 modes are Raman active, i.e.:

$$2A_{1g} + 4B_{1g} + 1B_{2g} + 5E_g \quad (1)$$

seven modes are IR active, i.e.:

$$3A_{2u} + 4E_u \quad (2)$$

the remaining ones are silent modes, i.e.:

$$1A_{2g} + 1A_{1u} + 1B_{1u} + 2B_{2u} \quad (3)$$

The scattering tensors of the Raman-active modes are reported in Ref.[16] According to the form of these scattering tensors, in order to discriminate among the A_{1g}, B_{1g}, B_{2g}, and E_g modes, it is necessary to accurately control the polarization direction of the incident and scattered light with respect to the a, b, c crystallographic axes (usually referred as the x, y, z axes of the intrinsic coordinate system).

Now, the determination of the c-axis direction can be easily achieved, thanks to the anisotropy of $LuPO_4$ uniaxial single crystal. However, the knowledge of the direction of the principal c-axis alone is insufficient to successfully explore all the possible symmetries of Raman active modes of $LuPO_4$, and the directions of the two equivalent a and b axes must be also known if confusion over assignment of some bands in its Raman spectrum is to be avoided. In our case, the proper orientation of the single crystal in the basal x-y plane was obtained using the micro-manipulator operated under direct visual control. Unfortunately, due to strong birefringence of the $LuPO_4$ crystal and to related depolarization effects, the measurement approach in backscattering geometry was not successful, because the impossibility to control the laser polarization direction inside the crystal. In fact, the depolarization of the laser radiation within the crystal gives rise to substantial spill-over effects of forbidden modes which appear in the experimental spectrum together with the allowed ones, thus preventing the identification of modes with the expected symmetry. However, this problem can be adequately overcome by exploiting the 90° scattering geometry, which constitutes an unusual scattering configuration for micro-Raman spectroscopy measurements. Through this innovative approach, it is possible to align the electric field of the incident radiation along the optical axis of the objective used to collect the scattered radiation, thus definitely improving the selectivity in symmetry. In brief, by alternatively exploiting the two measurement configurations, i.e. backscattering or 90° scattering geometry, highly selective Raman spectra of A_{1g}, E_g, B_{1g}, or B_{2g} symmetry can be recorded in turn on the properly oriented single crystal by simply varying the polarization direction of the scattered radiation.

The experimental micro-Raman spectra plotted in Fig. 1 were recorded either in backscattering (see panels a, b, and d) or under 90° scattering geometry (see panel c) without manipulating the polarization of the incident laser beam. The α_{YY}, α_{YX}, and α_{ZX} components of the Raman tensor in the laboratory coordinate system can be expressed in terms of the linear combination of α_{xx}, α_{yy}, α_{zz}, α_{xz}, and α_{xy} components of the Raman tensor in the intrinsic coordinate system, as follows:

$$a_{YY} = \sin^2\theta\alpha_{xx} + \cos^2\theta\alpha_{zz} - 2\sin\theta\cos\theta\alpha_{xz} \quad (4)$$

$$a_{YX} = \sin\theta\cos\theta\alpha_{zz} + \cos^2\theta\alpha_{zx} - \sin^2\theta\alpha_{xz} - \cos\theta\sin\theta\alpha_{xx} \quad (5)$$

$$\alpha_{ZX} = \sin\theta\cos\theta\alpha_{xx} + \cos^2\theta\alpha_{yx} - \sin^2\theta\alpha_{xy} - \cos\theta\sin\theta\alpha_{yy} \quad (6)$$

$$\alpha_{YX} = \sin\theta\cos\theta\alpha_{xx} + \cos^2\theta\alpha_{yx} - \sin^2\theta\alpha_{xy} - \cos\theta\sin\theta\alpha_{yy} \quad (7)$$

Equations (4)–(7) allow to evaluate the intensity variations, observed either in backscattering (Eqns (4), (5), and (7)) or in 90° scattering (Eqn (6)) geometries, of the different Raman modes as a function of the angle θ between the axes of the L-system and the intrinsic axes of the crystal.

Hence, for instance, the A_{1g} Raman modes can be selected, in back-scattering geometry, when the direction of the electric field of incident radiation is along the *c*-axis of the crystal, coincident with the Y direction of the L system (properly specified in the panel (a) of Fig. 1). As shown in Fig. 1, the observed A_{1g} spectrum of $LuPO_4$ consists of two intense Raman modes, peaked at about 490 cm^{-1} and 1010 cm^{-1}, respectively.

Journal of RAMAN SPECTROSCOPY

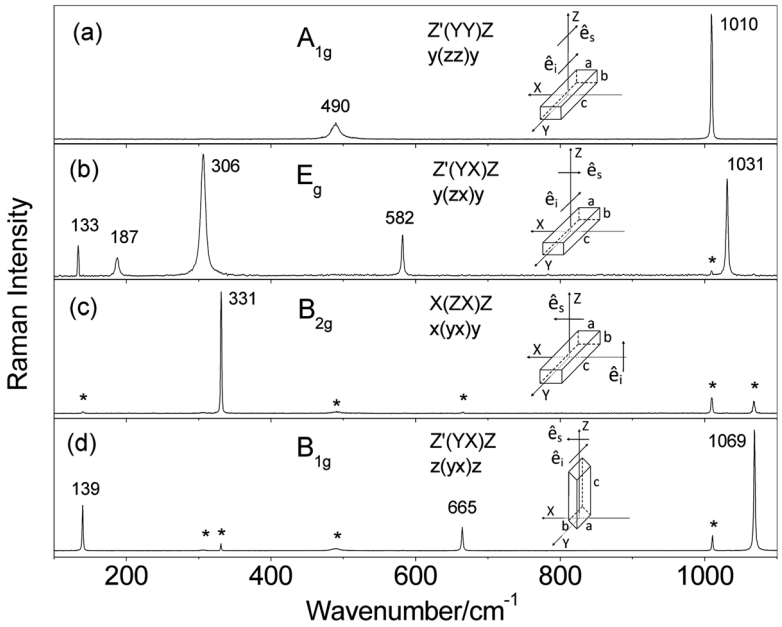

Figure 1. As-recorded polarized micro-Raman spectra of LuPO4 obtained in backscattering geometry (panels (a), (b), (d)) and in 90° scattering geometry (panel (c)) for different polarization and orientation settings, as sketched in each panel. For sake of clarity, the corresponding Porto's notation (uppercase letters refer to L-system, lowercase letters to C-system) is also reported. The stars (*) label the forbidden modes spilling over in the selected scattering configuration.

For the same crystal orientation by setting the analyser in crossed polarization, the E_g Raman modes can be displayed (panel(b)). In fact, the E_g spectrum, associated to the intrinsic α_{xz} and α_{yz} components of the Raman tensor (or to their linear combination as well), can be selected when the scattered radiation is analysed along the X direction, perpendicular to the crystallographic *c*-axis (as specified in the inset of panel (b)). As expected, on the basis of group theory, this spectrum consists of five vibrational modes, peaked at about 133 cm^{-1}, 187 cm^{-1}, 306 cm^{-1}, 582 cm^{-1}, and 1031 cm^{-1}, respectively.

On the other hand, under 90° scattering geometry, the B_{2g} Raman mode, associated to the intrinsic α_{xy} or α_{yx} component of the Raman tensor, is observed when the scattered radiation is analysed along the direction perpendicular to *c*-axis, i.e. when the electric field direction of the scattered radiation belongs to the basal x-y plane of the crystal. In order to get it, the crystal was held in the same orientation, but the 90° scattering geometry was exploited. Panel (c) of Fig. 1 shows the B_{2g} Raman spectrum, which consists of one very sharp line peaked at about 331 cm^{-1}.

Unfortunately, for this sample orientation, the pure B_{1g} spectrum cannot be straightforwardly obtained under the 90° scattering geometry, due to the difficulty to perfectly align the crystallographic a (or b) axis of the basal plane along the polarization direction of the incident radiation. Therefore, in order to measure the B_{1g} spectrum, the sample was preliminarily oriented with its crystallographic c-axis parallel to optical axis of the objective used to collect the scattered radiation (i.e.: Z axis of L system), and the backscattering geometry was adopted once again. The matching between the polarization direction of the incident radiation and the sample orientation in the basal plane was obtained by rotating step-by-step the crystal around its *c*-axis, until the Raman signal turned out maximized. The experimental spectrum measured in crossed polarization configuration, under the scattering conditions just outlined, is plotted in panel (d): three distinct Raman modes of B_{1g} symmetry, instead of the four expected on the basis of group theory, are clearly observable at 139 cm^{-1}, 665 cm^{-1}, and 1069 cm^{-1}, respectively, in fairly good agreement with the results of previous investigations.[11,20]

Ab initio calculations

Pure density-functional theory calculations with the use of effective core pseudo-potential have been performed to calculate the Γ-point phonon frequencies of $LuPO_4$, i.e. Raman, infrared, and silent vibrational modes. To the best of our knowledge, the vibrational properties of $LuPO_4$ have never been studied by means of *ab initio* methods. The present study has been made with the use of the CRYSTAL06 program,[21] a periodic *ab initio* code that uses a Gaussian-type basis set to represent the crystalline orbitals. All-electron basis sets have been used for phosphorus and oxygen atoms, with 85-21d1 (one s, three sp, and one d shell) contractions for the first one,[22] 6-31d1 (one s, two sp, and one d shell) contractions for the second one,[23] respectively. For lutetium atoms, quasi-relativistic effective core potential (60 electrons in the core) by Stuttgart-Cologne group has been adopted in order to reduce the computational effort and take into account the relativistic effects for the core electrons.[24,25] The 7-76d5 contractions (two s, one p, and one d shell) have been used for the valence electrons. More details on basis sets and computational parameters can be found at the CRYSTAL website.[26]

Following previous *ab initio* studies of the vibrational dynamics of isostructural orthophosphates,[16] Perdew-Becke-Ernzerhof exchange and correlation functionals have been utilized.[27] The truncation criteria in evaluating bielectronic integrals (Coulomb and exchange series) is set to standard values (6 6 6 6 12). The Monkhorst-Pack 8×8×8 *k*-point mesh in the Brillouin Zone was used.[28] The tolerance convergence threshold on the self-consistent field cycles was set to 10^{-7} Hartree for both total energy and eigenvalues, in order to ensure good convergence. The vibrational frequencies at the Γ point are calculated within the harmonic approximation

Table 1. Experimental and calculated optical phonon wavenumbers (cm^{-1}) of $LuPO_4$ at the Γ point. Column (a) refers to the *ab initio* calculations performed in this work, column (b) to our Raman measurements, column (c) to the experimental data reported in Refs [10,20]

Raman modes	Theory (a)	Exp. (b)	Exp. (c)
$E_g(1)$	134	133	144
$B_{1g}(1)$	146	139	138
$E_g(2)$	216	187	191
$E_g(3)$	308	306	308
B_{2g}	317	331	334
$B_{1g}(2)$	321	-	-
$A_{1g}(1)$	494	490	493
$E_g(4)$	552	582	587
$B_{1g}(3)$	650	665	670
$A_{1g}(2)$	1004	1010	1011
$E_g(5)$	1017	1031	1032
$B_{1g}(4)$	1051	1069	1069
Infrared modes	Theory (a)		Exp. (c)
$E_u(1)$	226		207
$A_{2u}(1)$	274		266
$E_u(2)$	351		347
$E_u(3)$	485		517
$A_{2u}(2)$	618		634
$E_u(4)$	981		1000
$A_{2u}(3)$	1050		1062
Silent modes	Theory (a)		
B_{1u}	157		
A_{2g}	250		
A_{1u}	410		
$B_{2u}(1)$	553		
$B_{2u}(2)$	981		

by diagonalizing the mass–weight Hessian matrix, whose (*i,j*) element is defined as $W_{ij} = H_{ij}/\sqrt{M_i M_j}$, where M_i and M_j are the masses of the atoms associated with the *i* and *j* coordinates, respectively. A more detailed description of the method and computational aspects can be found in Refs.[29,30]

The geometry optimization gives the cell parameters a = b = 6.8824 Å, c = 6.0402 Å, and a/c = 1.139, which differ from the experimental values [31] by about 1.4, 1.5, and 0.2%, respectively. These cell parameters have been used in the calculation of the vibrational frequencies reported below.

The calculated wavenumbers of the Raman and infrared modes of $LuPO_4$, compared with the available experimental data, including the new Raman results obtained in this work, are listed in Table 1. For completeness, the wavenumbers of the silent modes are also reported. The comparison between calculated (ν^{cal}) and experimental (ν^{exp}) frequencies, expressed in cm^{-1}, has been made through two parameters: (1) the average absolute difference and (2) the average of the relative differences (in percentage), both defined in the footnote.[1] We have considered as experimental wavenumbers ν^{exp} the average of the available experimental data, i.e. the average values of the columns (*b*) and (*c*). The obtained values for these two parameters, about 14.3 cm^{-1} and 3.6 %, respectively, show the very good agreement between calculated and experimental frequencies. In particular, the wavenumber of the missing $B_{1g}(2)$ Raman mode, never reported in literature, is computed at about 321 cm^{-1}. Accordingly to reduced-mass ratio considerations, carried out with respect to the wavenumber of $B_{1g}(2)$ mode of $ScPO_4$ and YPO_4 isomorphs, the experimental values of which are reported in Ref[16], the expected wavenumber value for this mode should fall nearby 300 cm^{-1} (see Fig. 2). Therefore, we can definitively conclude that the detection of this mode is masked by the spill-over of the $E_g(3)$ mode peaked at about 306 cm^{-1}.

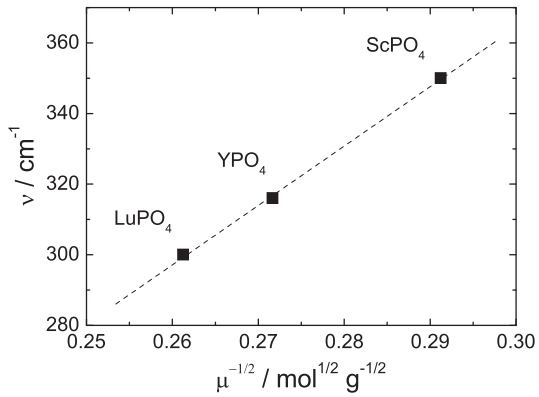

Figure 2. Wavenumber of B1g(2) mode in ScPO4, YPO4, and LuPO4, plotted *versus* the inverse of the reduced-mass square root of the R–O pair, with R = Sc, P, and Lu. The wavenumber values for ScPO4 and YPO4 plotted in the graph are taken from Ref [16] and are 350 and 316 cm^{-1}, respectively, while the wavenumber for LuPO4, estimated by means of the linear interpolation of the above experimental values, is close to 300 cm^{-1}.

Conclusions

In this work, 11 of the 12 allowed Raman modes of $LuPO_4$ have been selected in turn and assigned in symmetry by means of a proper polarization analysis of the Raman spectrum of this compound. With the aim of computing the Raman and infrared vibrational frequencies, *ab initio* calculations have been performed using an effective core potential for Lu and all-electron basis sets for P and O. The agreement between computational and experimental frequencies is very good. In particular, the wavenumber of the missing $B_{1g}(2)$ mode is computed at about 321 cm^{-1}. On the basis of *ab initio* results and of reduced-mass ratio considerations, it is concluded that the experimental evidence of the $B_{1g}(2)$ mode is hidden by the spill-over of the $E_g(3)$ mode peaked at about 306 cm^{-1}.

Acknowledgement

The research was partially funded by the Fondazione Cariverona (Verona, Italy), through a contract with the University of Verona.

References

[1] L. A. Boatner, G. W. Beall, M. M. Abraham, C. B. Finch, P. G. Huray, M. Rappaz EPR investigations of Gd3+ in single crystals and powders of the zircon structure orthophosphates YPO4 ScPO4 and LuPO4; Plenum: New York, **1980**.

[1]The average absolute difference and the average of the relative differences (in percentage) are defined as $\overline{|\Delta|} = \frac{1}{N}\sum_{i=1}^{N}\left|\nu_i^{cal} - \nu_i^{exp}\right|$ and $\overline{|\Delta_r|\%} = \frac{100}{N}\sum_{i=1}^{N}\left|\frac{\nu_i^{cal} - \nu_i^{exp}}{\nu_i^{exp}}\right|$, respectively, where $i = 1,\ldots,N$ indicates the 18 optical modes listed in Table 1.

[2] R. C. Ewing *Science* **1976**; *192*, 1336.
[3] T. Hayhurst, G. Shalimoff, N. Edelstin, L. A. Boatner, M. M. Abraham *J. Chem. Phys.* **1981**; *74*, 5449.
[4] J. O. Nriagu, P. B. Moore, F. Betts (eds.) Phosphate Minerals, Springer-Verlag, Berlin, **1984**.
[5] L. A. Boatner *Rev. Mineral. Geochem.* **2002**; *48*, 87.
[6] F. X. Zhang, M. Lang, R. C. Ewing, J. Lian, Z. W. Wang, J. Hu, L. A. Boatner *J. Solid State Chem.* **2008**; *181*, 2633.
[7] A. Tatsi, E. Stavrou, Y. C. Boulmetis, A. G. Kontos, Y. S. Raptis, C. Raptis *J. Phys. Condens. Mater.* **2008**; *20*, 425216.
[8] F. X. Zhang, J. W. Wang, M. Lang, J. M. Zhang, R. C. Ewing, L. A. Boatner *Phys. Rev. B* **2009**; *80*, 184114.
[9] A. N. Lazarev, N. A. Mazhenov, A. P. Mirgorodskii *Izvest. Akad. Nauk SSSR Neorgan. Mater.* **1978**; *14*, 2107.
[10] G. M. Begun, G. W. Beall, L. A. Boatner, W. J. Gregor *J. Raman Spectrosc.* **1981**; *11*, 273.
[11] A. Meldrum, L. A. Boatner, R. C. Ewing *Mineral Mag.* **2000**; *64*, 185.
[12] K. A. Farley *Geochim. Cosmochim Acta.* **2007**; *71*, 4015.
[13] R. Lacomba-Perales, D. Errandonea, Y. Meng, M. Bettinelli *Phys. Rev. B* **2010**; *81*, 064113.
[14] J. Lopez-Solano, P. Rodriguez-Hernandez, A. Munoz, O. Gomis, D. Santamaria-Perez, D. Errandonea, F. J. Manjon, R. S. Kumar, E. Stavrou, C. Raptis *Phys. Rev. B* **2010**; *81*, 144126.
[15] R. Mittal, S. L. Chaplot, N. Choudhury, C. K. Loong *J. Phys. Condens. Mater.* **2007**; *19*, 446202.
[16] M. Giarola, A. Sanson, A. Rahman, G. Mariotto, M. Bettinelli, A. Speghini, E. Cazzanelli *Phys. Rev. B* **2011**; *83*, 224302.
[17] R. S. Feigelson *J. Am. Ceram. Soc.* **1964**; *47*, 257.
[18] T. Damen, S. Porto, B. Tell *Phys. Rev.* **1966**; *142*, 570.
[19] W. O. Milligan, D. F. Mullica, G. W. Beall, L. A. Boatner Inorg *Chim. Acta.* **1982**; *60*, 39.
[20] A. Armbruster *J. Phys. Chem. Solids* **1976**; *37*, 321.
[21] R. Dovesi, V. R. Saunders, C. Roetti, R. Orlando, C. M. Zicovich-Wilson, F. Pascale, K. Doll, N. M. Harrison, B. Civalleri, I. J. Bush, P. DArco, M. Llunell Crystal06 User's Manual, University of Torino, **2006**.
[22] C. M. Zicovich-Wilson, A. Bert, C. Roetti, R. Dovesi, V. R. Saunders *J. Chem. Phys.* **2002**; *116*, 1120.
[23] M. Corno, C. Busco, B. Civalleri, P. Ugliengo *Phys. Chem. Chem. Phys.* **2006**; *8*, 2464.
[24] M. Dolg, H. Stoll, A. Savin, H. Preuss *Theor. Chim. Acta* **1989**; *75*, 173.
[25] http://www.theochem.uni-stuttgart.de/pseudopotentials/clickpse.en.html
[26] http://www.crystal.unito.it/
[27] J. P. Perdew, K. Burke, M. Ernzerhof *Phys. Rev. Lett.* **1996**; *77*, 3865.
[28] H. J. Monkhorst, J. D. Pack *Phys. Rev. B.* **1976**; *13*, 5188.
[29] C. M. Zicovich-Wilson, F. Pascale, C. Roetti, V. R. Saunders, R. Orlando, R. Dovesi *J. Comput. Chem.* **2004**; *25*, 1873.
[30] F. Pascale, C. M. Zicovich-Wilson, F. L. Gejo, B. Civalleri, R. Orlando, R. Dovesi *J. Comput. Chem.* **2004**; *25*, 888.
[31] S. J. Patwe, S. N. Achary, A. K. Tyagi *Am. Mineral.* **2009**; *94*, 98.